A Study on Automatic Disease Stage Classification for Glioma Histopathological Tissue Images

Kiichi Fukuma

A thesis submitted in partial fulfillment for the
Master degree in Engineering

in the

Graduate School of Engineering,
Mie University

Supervisor: Assoc. Prof. Haruhiko Takase

March 2017

Contents

List of Figures

List of Tables

Chapter 1

Introduction

1.1 Background

Recent studies in histopathology have made promising developments for analysis that would enable precision medicine and patient specific diagnosis [1, 2, 3, 4, 5, 6]. In typical clinical practice, medical doctors or pathologists manually analyze histopathological[1] images leading to a diagnosis. However, depending only on manual analysis has several problems. First, the number of images for a patient of tissue samples is typically large that becomes a burden when the pathologists manually analyze them. In certain cases, they have time constraints since the diagnosis is taking place during surgery. The combination of large number of images to be analyzed and time pressure for quick diagnosis places a heavy burden on clinical pathologists. Second, the criteria for diagnosis are not standard. Evaluation criteria heavily depends on the experiences and subjectiveness of each medical doctor or pathologist. Therefore, the results of the analysis are usually not quantitative. For these reasons, new and efficient methods that could automate and standardize the overall process would enable quick, efficient, and quantitative diagnosis is highly desired.

Many recent developments in biomedical informatics use computer vision techniques for computational pathology. These research reports show progress towards the goals for quick, efficient and quantitative analysis [1, 2, 3, 4, 5, 6]. In one such study [1], computer-assisted diagnosis (CAD) systems have been used to detect tumors from histopathological tissue images. This method was required strong feature extraction and further classification analysis to determine the prognosis of a patient. Feature descriptors were employed for effective cytopathology and histopathology. However, many of the previous research works mainly applied these methods to some specific diseases, like breast cancer, or esophagitis, and or not widely applied to other areas such as the brain yet. In addition, the breast cancer and esophagitis

[1] the branch of medical science that studies the causes and nature and effects of diseases.

reports were focused on research in the field of histopathology and not yet widely applied in clinical practice as well.

Based on these observations, the focus of this study was on Glioma histopathological images. Glioma is one of the most malignant tumors occurring in the brain. The prognosis of Glioma is usually quite poor in clinical practice. A system that would utilize automation towards aiding disease stage classification of Glioma would benefit greatly in predicting a timely diagnosis, which could aid appropriate treatment and in turn enhance patient outcome greatly.

The approach of this study was to apply methods of biomedical informatics to Glioma histopathological images. There are many feature descriptors that can be used to analysis histopathological images. However, most of these feature descriptors have been, so far, applied only to other diseases such as breast cancer. Therefore, the effectiveness of the standard features such as the spatial, textural, regional feature descriptors for Glioma is not yet known. Part of this work was to check the effectiveness of these feature descriptors for Glioma histopathological images. The checked descriptors have been reported as useful in previous research works for other tissue types. Therefore, I have decided to check the effectiveness of certain feature descriptors for Glioma histopathological images. The results were reported in [7, 8].

1.2 Objective

The objective of this study is automatic disease stage classification of Glioma histopathological images. The secondary objective is to determine the effectiveness of this method using multiple image sets. The prior study used only 1 pair image set, High grade and Low grade [9]. This work discusses

- Method of nuclei segmentation using custom-designed image processing
- Performance of this segmentation method
- Various feature descriptors which are then used to evaluate and disease stages classification of Glioma

The images used for analysis in this study were obtained from The Cancer Genome Atlas (TCGA) [11]. Significant feature descriptors for Glioma images were determined and used for classification using Support Vector Machine (SVM) and Random Forests (RF) [10]. This thesis shows that the proposed image analysis pipeline can be used effectively in feature extraction and disease stage classification for Glioma histopathological images. Further, the pipeline is general in the sense that it is extensible to other tissue type images.

Rest of the thesis is organized as follows. Chapter 2 and Chapter 3 compare the performance of the proposed method with other segmentation schemes. Chapter 4 shows the experimental results and has a discussion. Finally, Chapter 5 concludes the study.

Chapter 2

Materials

2.1 Histopathological Images of Glioma

In this study, I used human brain histopathological images of Glioma. Generally, Glioma can be categorized into four grades based on their disease stage. For example, Glioma of Grade 1 has a slight illness, and Grade 4 is so serious and has a poor prognosis. In particular, the average life expectancy of Grade 4 is one and half year in general. Figure 2.1 shows an example of histopathological images. As shown the figure, the histopathological images are dominated by regions with many cell nuclei and cytoplasm. Some images contain other structures or tissue types, such as vessels, and blood cells. In the figure, the objects stained deep purple are cell nuclei, the objects stained bright red are blood cells, and the light colored regions are primarily cytoplasm.

As seen in Figure 2.1, the grade of the disease progression seems to correlate with some image features, such as nuclei properties of size, shapes, density and typology about other nuclei. Therefore, these features in the images were used for analysis in the study of biomedical informatics.

2.2 Obtained Images

The images used in this study were obtained from the publicly available The Cancer Genome Atlas [11] (TCGA) database. This database has many histopathological images, such as Glioma, Breast Cancer, and Esophagitis. TCGA contains two types of images, *i.e.* Lower-Grade Glioma (LGG) and Glioblastoma multiforme (GBM). LGG includes images of Grade 1 and 2, GBM includes images of Grade 3 and 4. Certain attributes of the database of TCGA-LGG and TCGA-GBM are shown in Figure 2.2. In this study, these two distinct type images were used as the experimental imagery for automatic analysis. Figure 2.3 shows example images. In these

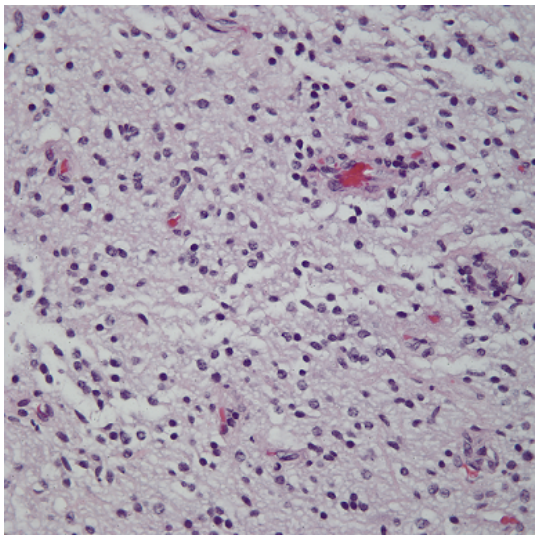

Figure 2.1: Example of a histopathological image.

images, the nuclei were stained deep purple, and other tissues were stained pale purple and red by Haematoxylin and Eosin (H&E) staining. Image features with respect to the nuclei appear different based on the grade, and features of the organization are different from each other. Generally, these differences are believed to result from the disease progression, including changes in gene and protein expression.

In the previous research [9], an image in each category, LGG and GBM was used. Then, the authors could only say that there were possibilities of being affected by not only disease stage but also differences of the staining states. Therefore, this thesis used 10 LGG images and 10 GBM images respectively to avoid this problem.

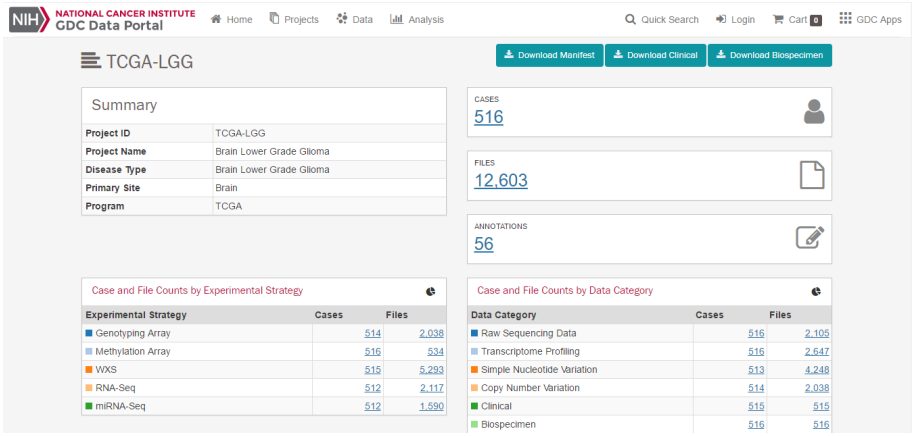

(a) TCGA-LGG

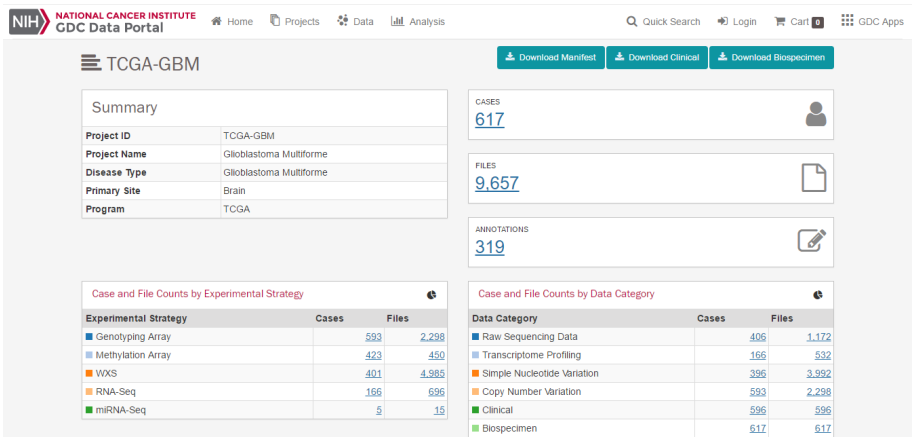

(b) TCGA-GBM

Figure 2.2: The Cancer Genome Atlas [11] (TCGA) database where the experimental histopathological imagery were acquired. (a) Lower-Grade Glioma (LGG), and (b) Glioblastoma multiforme (GBM) cases.

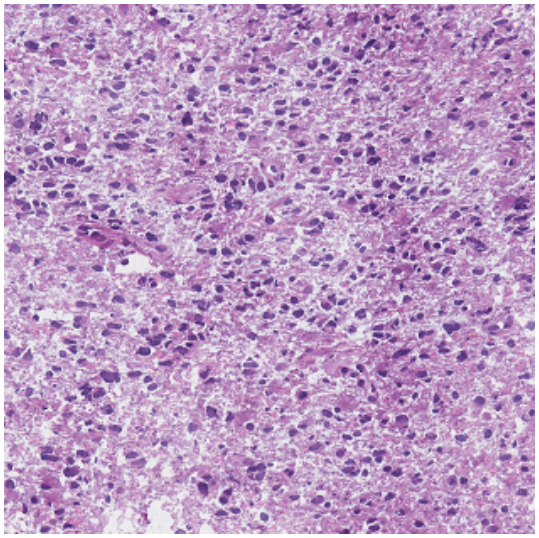

(a) Lower-Grade Glioma (LGG)

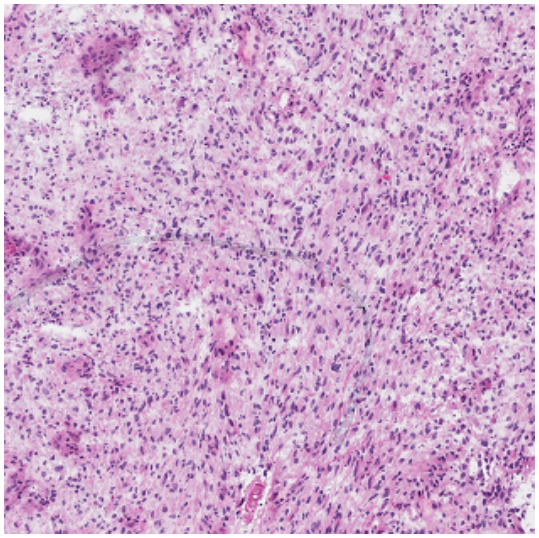

(b) High-Grade Glioma (GBM)

Figure 2.3: Samples of Glioma histopathological images. (a) Lower-Grade Glioma (LGG) and (b) High-Grade Glioma (GBM).

Chapter 3

Methods

The methods used in this study consist of four main steps (Figure 3.1): Data-set Construction, Nuclei Segmentation, Feature Extraction, and Classification. In the Classification step, Support Vector Machine (SVM) and Random Forest (RF) were used for efficient classification.

3.1 Data-set Construction

The first step of the methods is to construct the experimental data-set. The histopathological images of Glioma obtained from TCGA database were in the .svs format. These images are too large (approximately 30000×30000 pixels) to be used on the target computational platform, such as a standard personal computer/laptop. Sample images of original large scale LGG and GBM image files are shown in Figure 3.2. The original sized images were divided into patched images whose sizes were 2000×2000 pixels. These patched images were used as experimental materials. Figure 3.3 shows how the original images were divided into patched images

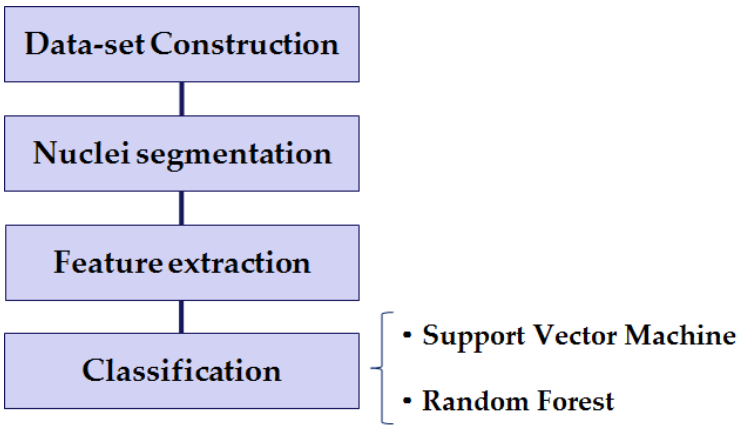

Figure 3.1: General procedure of experimental method.

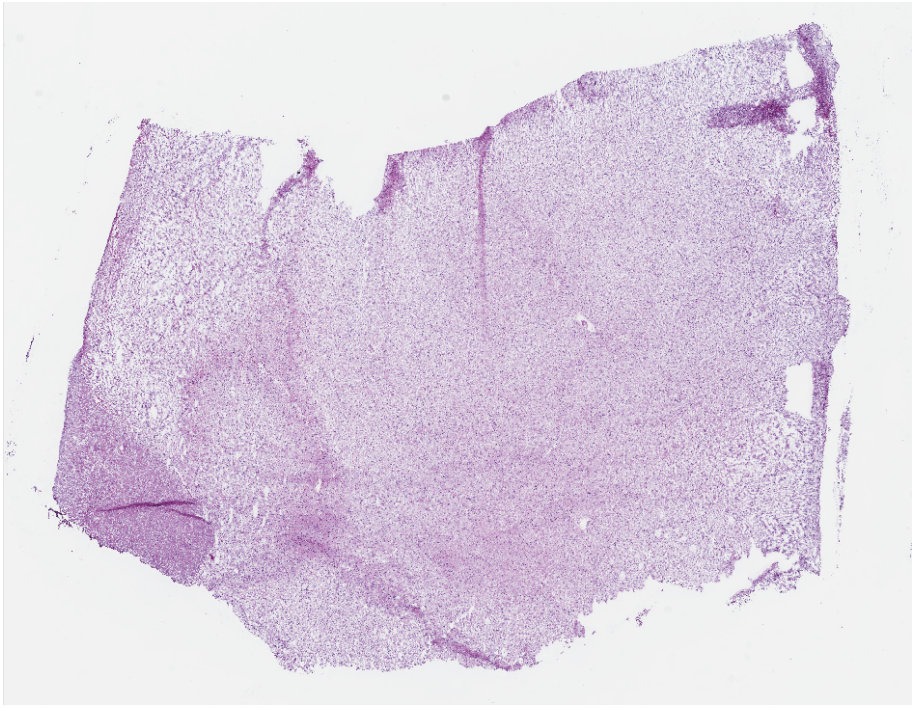

(a) LGG (40528 x 32125 pixels)

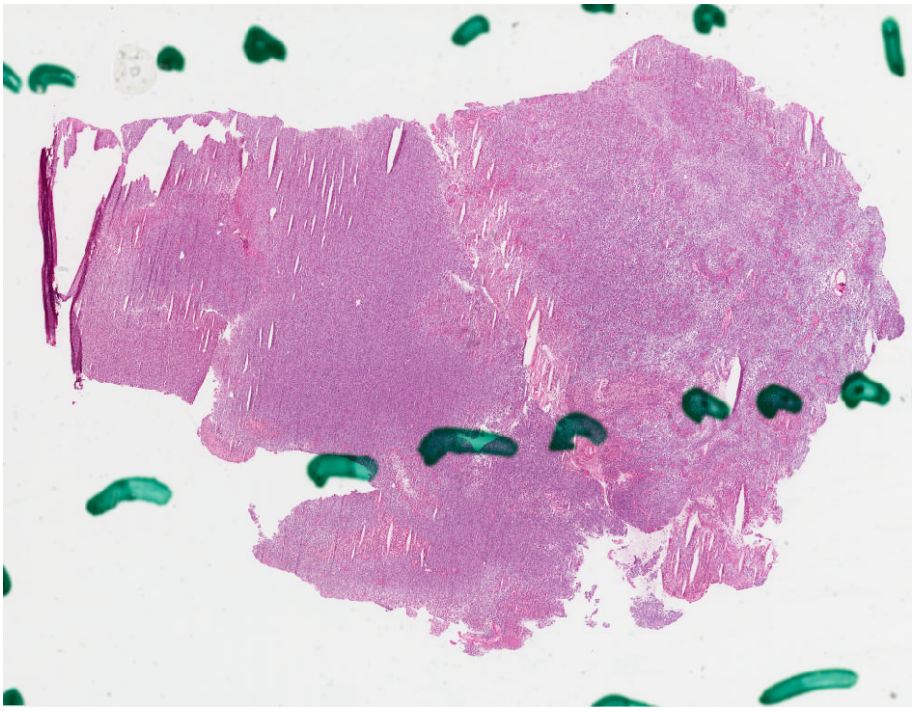

(b) GBM (39077 x 30186 pixels)

Figure 3.2: Samples of original large scale images from TCGA database. (a) Lower-Grade Glioma (LGG), and (b) High-Grade Glioma (GBM).

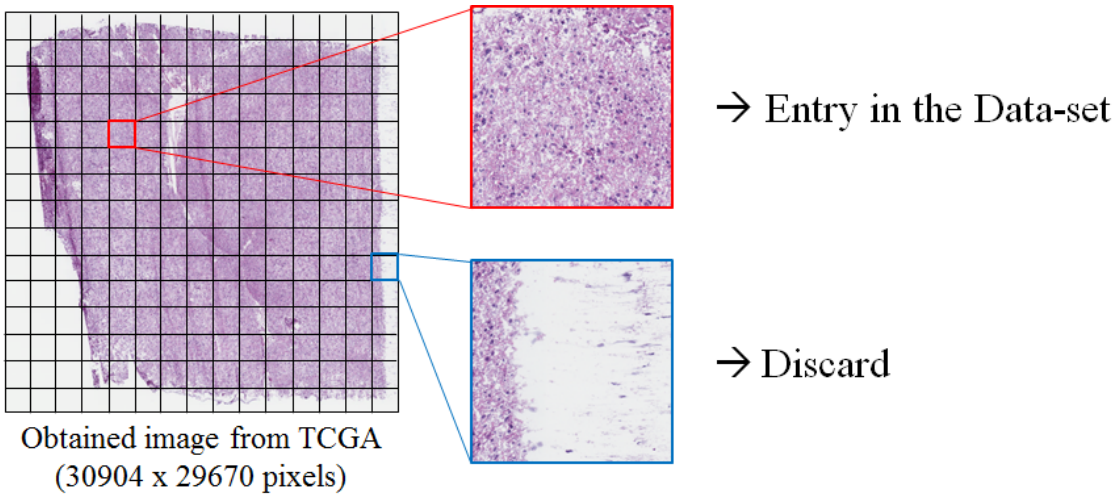

Figure 3.3: Criterion to divide the original histopathological image to small patches.

and the criteria. In the figure, a patched image, which was uniformly covered by the sufficient number of nuclei, were added to the data-set. For this study, 10 .svs format images in each category were used. From each original image, 100 patched images were made. Therefore, 1000 patched images in each category were used in this study.

3.2 Nuclei Segmentation

The second step of the method is Nuclei Segmentation. Nuclei properties were primary focused for the analysis because these properties change with the disease stage progression.

CellProfiler [12] was utilized in this study for image segmentation. CellProfiler is an open source library and it is designed for histopathology image processing. This software also supports basic methods and algorithms. Figure 3.4 shows the pipeline, the flow of processing steps, of this particular segmentation method. This pipeline consists of three main steps:

- Pre-processing (yellow)
- Rough segmentation (green)
- Nuclei separation (blue)

3.2.1 Pre-processing

The design for pre-processing is based on the characteristics of the H&E stained image. The goal is to isolate the nuclei and reduce the pixel memory during Pre-

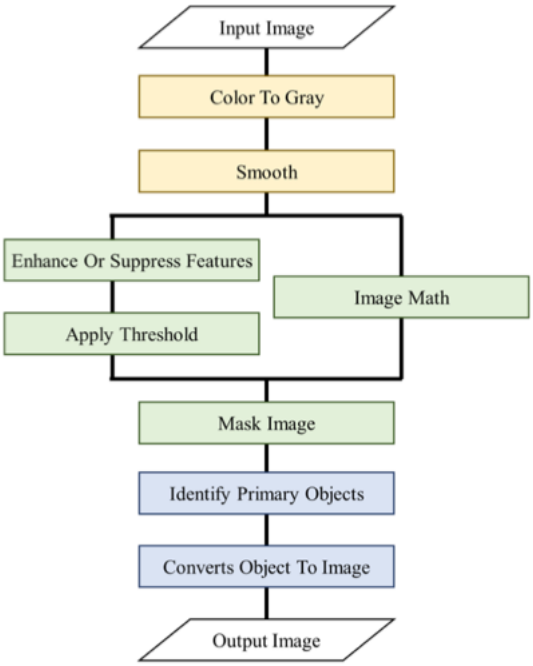

Figure 3.4: Segmentation pipeline used in the proposed method.

processing. If the colors of the H&E images is converted to gray-scale, the both dark purple nuclei and deep red blood vessels appear as dark spots. The separation is done as follows. The input image is converted to a gray-scale image by using Color To Gray module. The parameters of the module were set to illuminate red colored objects, *e.g.* blood cells.

And then, Smooth module smooths the converted image to remove artifacts of a particular size, like a bubble on the cell nuclei in the image. In this module, Smooth Keeping Edges is applied as a smoothing method. This method uses a bilateral filter which limits Gaussian smoothing across an edge while applying smoothing perpendicular to an edge. The effect is to respect edges in the image while smoothing other features. Figures 3.5 (a), (b) and (c) show input, gray-scale, and smoothed images, respectively. Fuzzy smoothing and adaptive thresholding techniques [13, 14] can be used to improve these preliminary pre-processing steps.

3.2.2 Region Extraction

Next, nuclei in the image is roughly segmented by using the following procedure. Enhance Or Suppress Features module was used to emphasize dark regions, *i.e.* nuclei. The module enhances or suppresses certain image features (such as speckles, ring shapes, and neurites), which improve subsequent identification of objects. This module enhances or suppresses the intensity of certain pixels about the rest of the image, by applying image processing filters. It produces a gray-scale image in which objects can be identified with Identify module. In this study, enhancing the objects

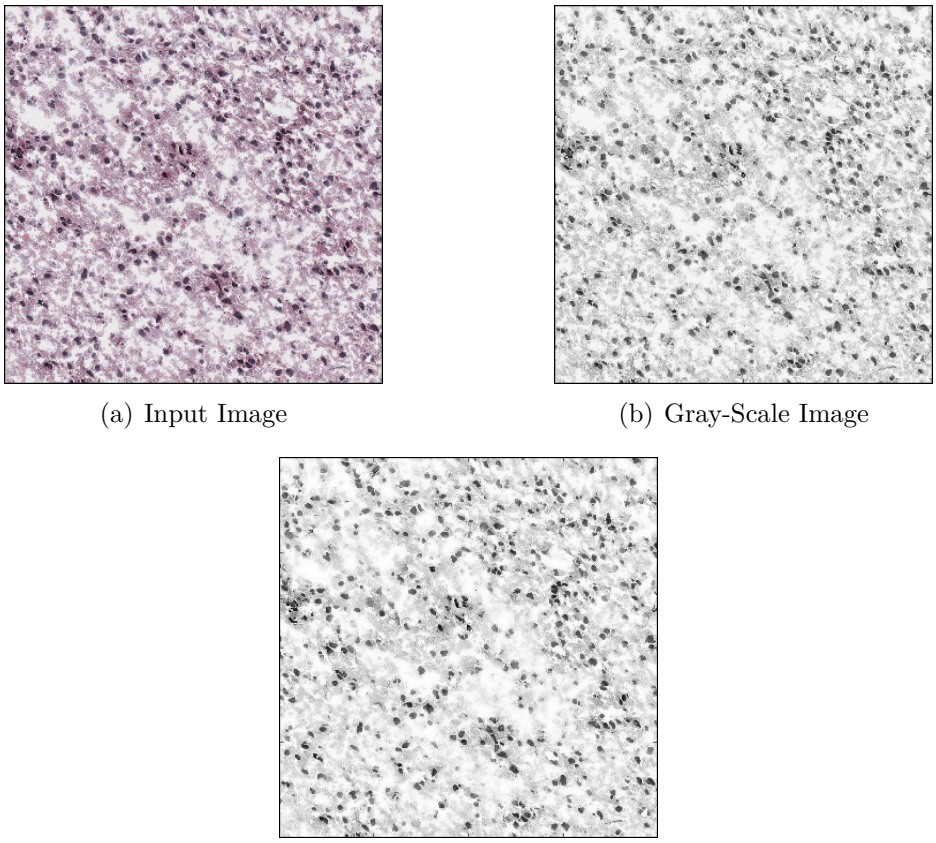

(a) Input Image

(b) Gray-Scale Image

(c) Smoothed Image

Figure 3.5: Pre-processing steps consist of gray-scale conversion and smoothing using bilateral filter.

(nuclei) is selected. Therefore, this module uses morphological reconstruction (the rolling-ball algorithm) to identify dark holes within brighter areas or brighter ring shapes. The image is inverted so that the dark holes turn into bright peaks. As a result, the inverted image shown in Figure 3.6 (a) is obtained.

After this, Apply Threshold module is used to obtain the binary image as shown in Figure 3.6 (b). Apply Threshold module produces either a gray-scale or binary image based on a threshold that is pre-selected or calculated automatically. In this study, output image type is a binary image. And threshold strategy is Adaptive and the image threshold is determined based on the pixel intensities. Adaptive partitions the input image into tiles and calculate thresholds for each tile. For each tile, the calculated threshold is applied only to the pixels within that tile. Thresholding method for binarizing is Otsu, this approach calculates the threshold to separate pixels (foreground and background) with discriminant analysis. As shown in Figure 3.6, the method can roughly extract nuclei regions from the obtained image, but adjacent nuclei are grouped as one nucleus.

To separate the adjacent nuclei regions, the inverted image is prepared without enhancement (Figure 3.6 (c)) by using Image Math module and the smoothed image

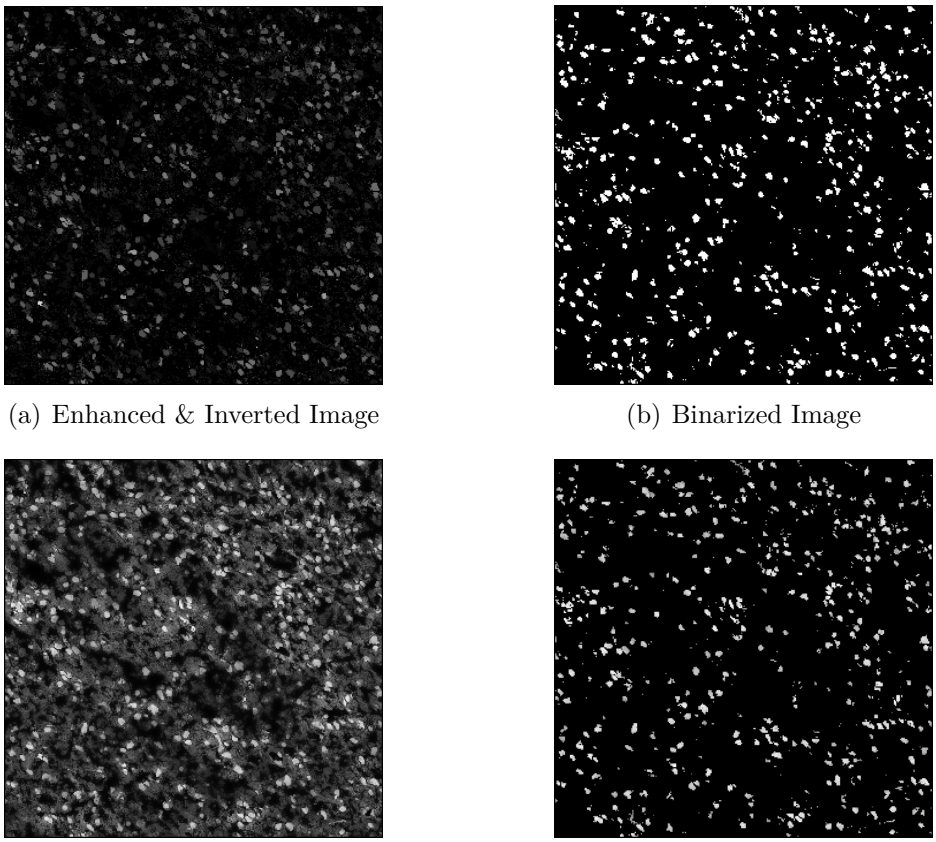

(a) Enhanced & Inverted Image

(b) Binarized Image

(c) Only Inverted Image

(d) Region Extracted Image

Figure 3.6: Example of rough segmentation step.

(Figure 3.5 (c)). In Image Math module, Invert is selected as an operation to perform. Invert subtracts the image intensities from 1. This makes the darkest color the brightest and vice-versa. Then, the rough segmented image was obtained by superimposing the binary image (Figure 3.6 (b)) and the inverted image (Figure 3.6 (c)). In this step, Mask Image module was employed to superimpose. Figure 3.6 (d) shows the result of rough segmentation by the above procedure.

3.2.3 Nuclei Separation

As the last step, adjacent nuclei regions are separated into each nucleus based on the distribution of pixel values. As seen in Figure 3.7, an adjacent nucleus region has plural peaks like a multimodal distribution. The typical distribution of pixel values of a single nucleus is unimodal. Thus, local minimum points of pixel values in the region were detected and Identify Primary Objects module is used to trace the points. Identify Primary Objects module identifies biological components of interest in gray-scale images that contain bright objects on a dark background. For using this module, the input image should have the following qualities. The image should be gray-scale, and the foreground (*i.e.* regions of interest) are lighter than

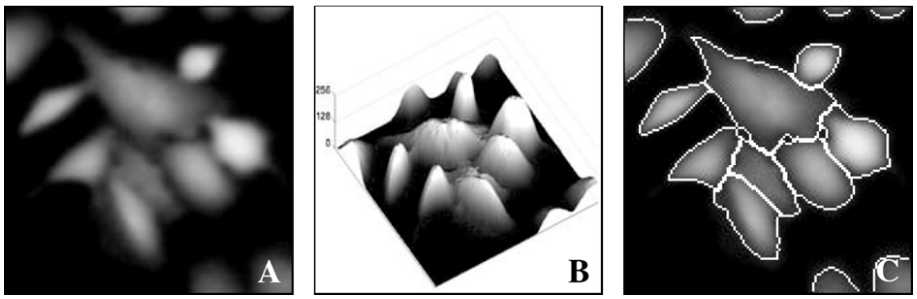

Figure 3.7: Basic overview of pixel values in the nuclei regions.

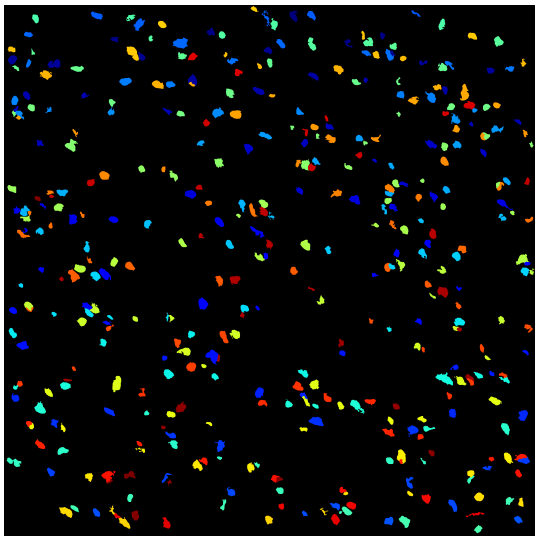

Figure 3.8: Segmentation result.

the background. And in this module, objects that touch the border of the image were removed. Removing objects that touch the image border is important for accurate analysis because morphological measurements obtained from a portion of an object will not be accurate. In this module, the method to distinguish clumped objects is Intensity. When this method is used and if the objects have some peaks of brightness, this option counts each peak point as a separate object and the object centers are defined as local intensity maximum in the smoothed image. Figure 3.7 shows the basic overview of this concept.

After that, each separated nucleus was colored for recognizing individual nucleus using Converts Object To Image module. Figure 3.8 shows the resulting segmented image.

3.3 Feature Extraction

Feature descriptors used to analyze histopathological images can be categorized into two types [1]:

- Object-Level features
- Spatial-Arrangement features

Both types were utilized in this study.

3.3.1 Object-Level Features

Object-Level features are directly related to the size and shape of each object, such as a nucleus. The outline around the region of each nucleus is expressed with one of these six types:

- Original nucleus
- Elliptical nucleus
- Convex Hull nucleus
- Bounding Box nucleus
- Boundary of nucleus

The examples of outline figures are shown in Figure 3.9. For the Original nucleus, Number of nuclei, Area of nucleus and other features are used as the feature descriptors (Figure 3.9 (a)). For the Elliptical nucleus, at first, an approximate ellipse around the original nucleus is generated (Figure 3.9 (b)). After that, the Major and Minor Axis Length, Eccentricity, Orientation, Elliptical Deviation, Extent and Aspect Ratio are calculated. In the same way, for the Convex Hull and Bounding Box of nucleus, the smallest convex hull object and smallest bounding box like Figure 3.9 (c) and (d) are made and then, some feature descriptors shown in Table 3.1 are extracted. Boundary of nucleus is related to the outline of original nucleus, and these feature descriptors are related to the perimeter of the nucleus (Figure 3.9 (e). All of the extracted Object-Level features are shown in Table 3.1.

3.3.2 Spatial-Arrangement Features

Spatial-Arrangement features are features with respect to the topographical position of nuclei. To get these features, a nucleus is called a node and graphs that connect the nodes are constructed [17, 18, 19]. For instance, B. Weyn used fractal and syntactic structure analysis (SSA), and he took into account the spatial-arrangement features [17]. Furthermore, he applied SSA to malignant mesothelioma images in [18]. Another report [19] shows a method to make perceptual boundaries of relatively homogeneous dot patterns. Generally, Spatial-Arrangement features do not depend on the shapes of segmented nuclei, but their positions and distances

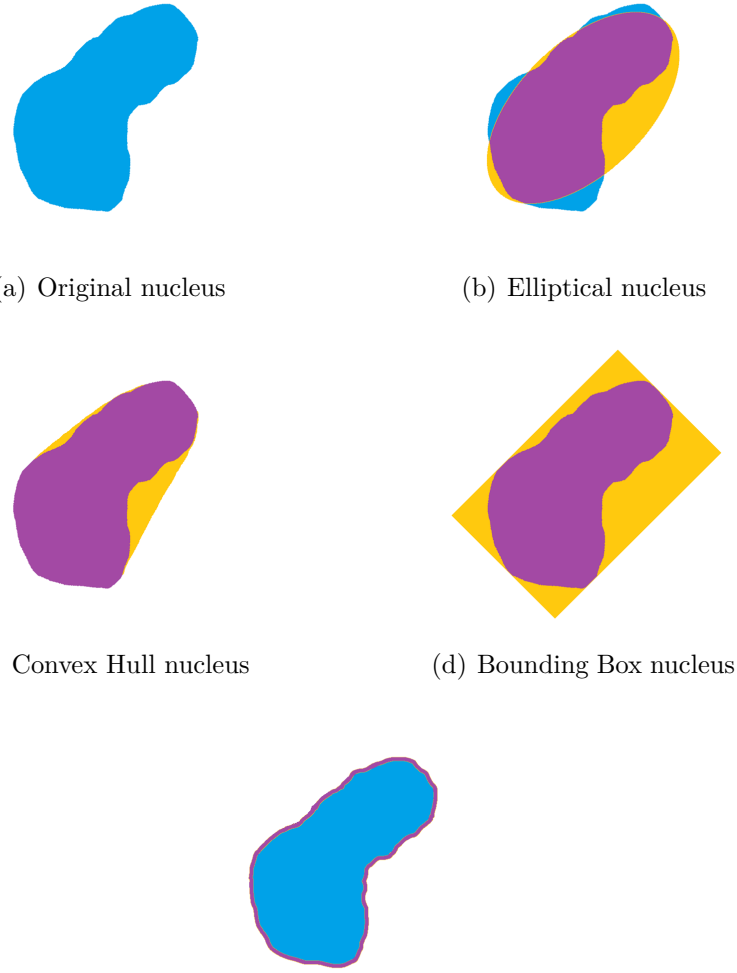

(a) Original nucleus

(b) Elliptical nucleus

(c) Convex Hull nucleus

(d) Bounding Box nucleus

(e) Boundary of nucleus

Figure 3.9: Outline figures of Object-Level features.

among nodes. Such topological features can be also valiant descriptors to express the Spatial-Arrangement of nodes.

In this study, the thesis uses three types graph as follows:

- Voronoi Tessellation (VT)
- Delaunay Triangulation (DT)
- Minimum Spanning Tree (MST)

These graphs are constructed from input images (segmented images). Samples of an input image and the constructed graphs are shown in Figure 3.10. Table 3.2 shows all of the extracted Spatial-Arrangement features [20].

These graphs are constructed as follows. First, Voronoi Tessellation is obtained from the input image. In the tessellation, the circle marks indicate the nodes lo-

Table 3.1: List of Object-Level features.

	Type	Features
Object-Level Features	—	# of nuclei, Area
	Elliptical	Major Axis Length Minor Axis Length Eccentricity Orientation Elliptical Deviation Extent Aspect Ratio
	Convex Hull	Convex Area Convex Deficiency Solidity
	Bounding Box	Extent Aspect Ratio
	Boundary	Perimeter Radii Perimeter Curvature
	Other Shape	Equivalent Diameter Sphericity Compactness Inertia Shape

cated at gravity centers of each of the nuclei. Then, the perpendicular bisectors of nodes are connected each other. The sample graph is shown in Figure 3.10 (b). As shown, the obtained graph has many regions that are surrounded by perpendicular bisectors. Therefore, the thesis extracts feature descriptors related to these regions from Voronoi Tessellation.

Next, the graphs of Delaunay Triangulation is constructed. The graphs of Delaunay Triangulation is constructed from the graphs of Voronoi Tessellation by connecting the nodes of the neighboring boundary region in Voronoi Tessellation. Therefore, it is expected that Delaunay Triangulation shows the adjacency relationship pf the Voronoi regions. The sample graph of Delaunay Triangulation is shown in Figure 3.10 (c).

This study also constructs the graphs of Minimum Spanning Tree (MST). MST is obtained by connecting all of the nodes in the graphs with the minimum edge length of Delaunay Triangulation. An example of Minimum Spanning Tree is shown at Figure 3.10 (d).

3.3.3 Kolmogorov-Smirnov (K-S) Test

The effectiveness of the above feature descriptors has already been confirmed in literature [9]. In the [9], the feature descriptors defined in the literature [1] were

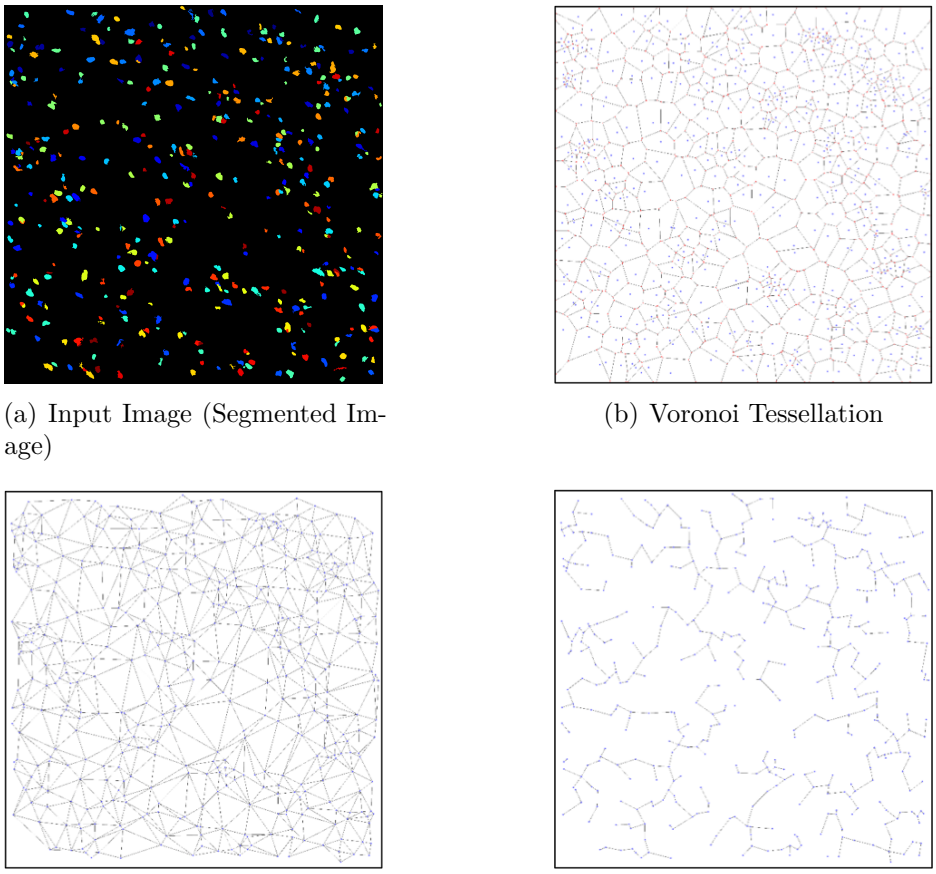

(a) Input Image (Segmented Image)

(b) Voronoi Tessellation

(c) Delaunay Triangulation

(d) Minimum Spanning Tree

Figure 3.10: Samples of input image and output graphs.

applied to the Glioma histopathological images in TCGA database, and their statistical significances were evaluated by using Kolmogorov-Smirnov (K-S) test. The significance level was set to 0.01.

Tables 3.3 and 3.4 show the summarized results on Object-Level and Spatial-Arrangement features, respectively. From the results, p-values of all feature descriptors were less than 0.01, and they all were regards as effective for evaluation of disease progression of Glioma.

3.4 Classification

The significant feature descriptors are employed to generate a feature vector for disease stage classification. In this study, all of the feature values obtained by significant descriptors were used as coefficients of the feature vectors. The patched images were classified by using Support Vector Machine (SVM) and Random Forests (RF). In this study, these classifiers were implemented by "R", which was a software for statistical analysis.

Table 3.2: List of Spatial-Arrangement features.

	Type	Features
Spatial-Arrangement Features	Voronoi Tessellation	# of Nodes # of Edges Edge Length Cyclomatic # # of k-Walks Degree Spectral Radius Randic Index Area Area Disorder Perimeter Roundness Factor Roundness Factor Homogeneity
	Delaunay Triangulation	# of Nodes # of Edges Edge Length Cyclomatic # # of Triangles # of k-Walks Degree Spectral Radius Randic Index
	Minimum Spanning Tree	# of Nodes # of Edges Edge Length Degree Spectral Radius Randic Index

3.4.1 Support Vector Machine

The data-set was divided into two subsets, testing data (10%) and parameter tuning and training data(90%). Then, the parameters of SVM was tuned with the tuning data. The classification result is affected by random sampling process in the data-set division. Therefore, classification test was done ten times and then, the average of the classification results was used for evaluation.

3.4.2 Random Forest

In the RF using R, the parameter m_{try} should be tuned. The parameter means the number of feature descriptors to be used to construct a decision tree for RF. The default parameter of $mtry$ is $\sqrt{n}$, and n is the number of feature descriptors for anal-

Table 3.3: Kolmogorov-Smirnov (K-S) test result of Object-Level features.

Type	Features	p-value
—	# of Nuclei	< 0.01
	Area	
Elliptical	Major Axis Length	< 0.01
	Minor Axis Length	
	Eccentricity	
	Orientation	
	Elliptical Deviation	
	Extent	
	Aspect Ratio	
Convex Hull	Convex Area	< 0.01
	Convex Deficiency	
	Solidity	
Bounding Box	Extent	< 0.01
	Aspect Ratio	
Boundary	Perimeter	< 0.01
	Radii	
	Perimeter Curvature	
Other Shape	Equivalent Diameter	< 0.01
	Sphericity	
	Compactness	
	Inertia Shape	

ysis. In this thesis, m_{try} was obtained by using $tuneRF$ function. Figure 3.11 shows the relationship between m_{try} and $OOB\ error$. RF was trained using bootstrap aggregation, where each new tree was fit from a bootstrap sample of the training observations z_i. $OOB\ error$ is the average error for each z_i that is calculated using predictions from the tree that do not contain z_i in their respective bootstrap sample. In the case of Figure 3.11, $m_{try} = 2$ is the best parameter and the value was used for experiments.

Table 3.4: Kolmogorov-Smirnov (K-S) test result of Spatial-Arrangement features.

Type	Features	p-value
Voronoi Tessellation	# of Nodes # of Edges Edge Length Cyclomatic # # of k-Walks Degree Spectral Radius Randic Index Voronoi Area Voronoi Area Disorder Perimeter Roundness Factor Roundness Factor Homogeneity	< 0.01
Delaunay Triangulation	# of Nodes # of Edges Edge Length Cyclomatic # # of Triangles # of k-Walks Degree Spectral Radius Randic Index	< 0.01
Minimum Spanning Tree	# of Nodes # of Edges Edge Length Degree Spectral Radius Randic Index	< 0.01

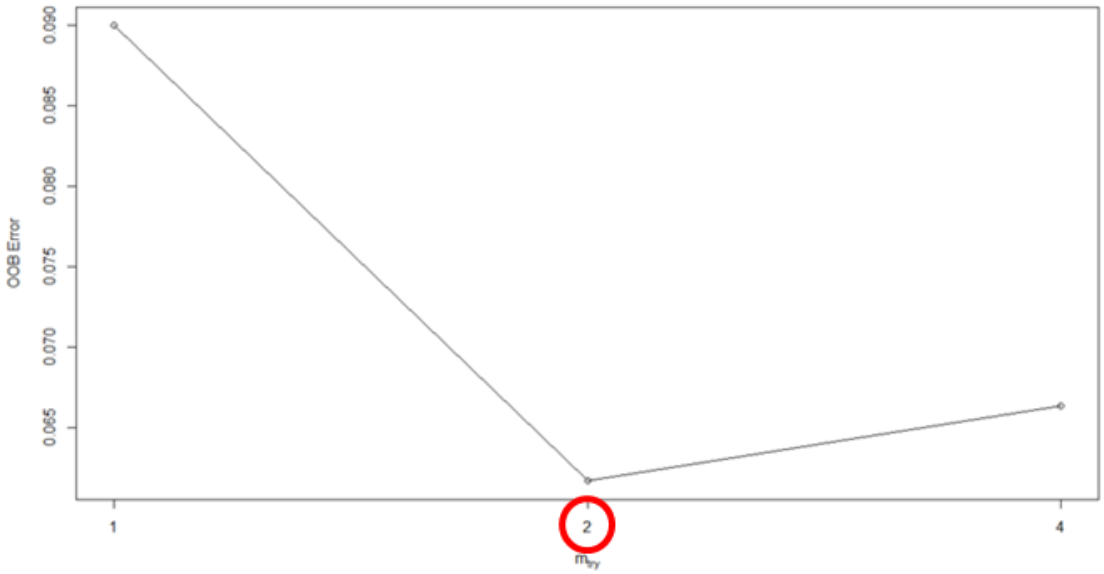

Figure 3.11: Sample result of *tuneRF* function.

Chapter 4

Results and Discussions

4.1 Results

4.1.1 Accuracy of Nuclei Segmentation Method

To verify the accuracy of the nuclei segmentation method, the segmented images were compared with manual-traced images. Since these manually traced images were generated under the guidance of experienced pathology professionals, the resulted images were regarded as grand-truth (GT) for the verification process and nuclei segmentation method.

Manual-traced Images

For proper evaluation of the segmentation method, manual-traced images that accurately isolate each nucleus are required. Under the guidance of pathologists, 4 types of small patched images were utilized to make the manual-traced images. This study employed five people to make them. The boundaries of nuclei in the image were traced with a stylus for a pen tablet device (LCD TABLET DTZ-1200W/G0, WACOM Co., Ltd.). After this, the manual-traced images were generated by using trajectories (stroke-data) of the stylus and coloring processing mentioned the above. Figure 4.1 (a) shows an example of small patched image, and (b) is a result example of the automatic nuclei segmentation. Figure 4.1 (c) is a generated manual-traced image.

Evaluation of Accuracy of Nuclei Segmentation

The accuracy of nuclei segmentation is evaluated with the following criteria.

- Accuracy of Area of each Nucleus is defined by

$$f_s = \sum_{N_a}\{100 - (\frac{|S_a - S_m|}{S_m} \times 100)\}.$$

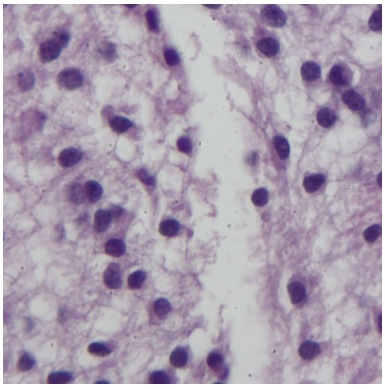

(a) Small Patched Image

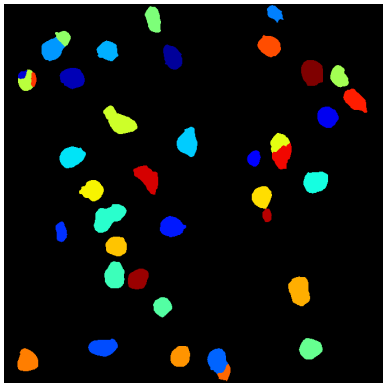

(b) Automatic Segmentation Image

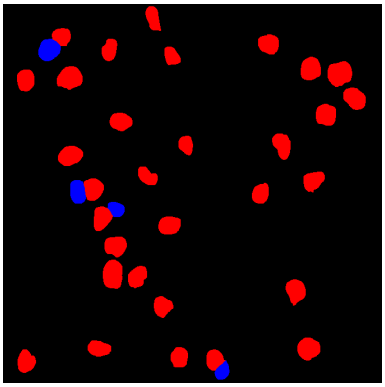

(c) Manual-traced Image

Figure 4.1: Sample images for evaluating the automatic nuclei segmentation accuracy.

N_a is the number of nodes, *i.e.* extracted nuclei by the automatic nuclei segmentation method. S_a is the area of an extracted nucleus by the automatic nuclei segmentation method, and S_m is the area of the corresponding manual-traced nucleus.

In addition, the following formula is also used.

- Accuracy of Number of Nuclei is defined by

$$f_n = 100 - (\frac{|N_a - N_m|}{N_m} \times 100).$$

N_a is the number of nuclei by the automatic nuclei segmentation method, and N_m is the number of the corresponding manual-traced nuclei.

The f_s and f_n percentages formulas reflect values determined by how the automatic segmentation results match to the manual segmentation results. If the result of automatic nuclei segmentation is completely matched to that of manual-traced

Table 4.1: Nuclei segmentation accuracy (f_s). For the area of corresponding nuclei.

	Image-1	Image-2	Image-3	Image-4
f_s[%]	84.7	89.9	81.4	79.7
Area Segmentation Accuracy Average 83.9[%]				

Table 4.2: Nuclei segmentation accuracy (f_n). For the number of identified nuclei.

	Image-1	Image-2	Image-3	Image-4
f_n[%]	86.6	84.8	81.4	99.4
Number Segmentation Accuracy Average 88.1[%]				

segmentation, f_s and f_n would be 100%. f_s and f_n were calculated for each manual-traced image.

Tables 4.1 and 4.2 show summarized results of segmentation accuracies on f_s and f_n. The averages of f_s and f_n were 83.9% and 88.1%, respectively. These accuracy values were sufficient for verification of the automatic segmentation procedure used in this study [15].

4.1.2 Support Vector Machine

Table 4.3 shows the results of disease stage classification using SVM. The obtained classification accuracy was 98.8% when all Object-Level features were used. This result indicates that most of Glioma histopathological images can be classified correctly with SVM and Object-Level features.

On the other hand, the results using VT and DT were 84.2% and 86.5%, respectively. In the case of MST, the obtained accuracy was 87.6%. And 87.8% of given images were classified correctly when all Spatial-Arrangement features were used. In addition, the result of all features, *i.e.* the both of Object-Level and Spatial-Arrangement features, was 96.5%.

4.1.3 Random Forest

Tablel 4.3 and Figures 4.2 show the result of disease stage classification using RF and graphs of Mean Decrease Gini. Mean Decrease Gini means importance for classification, and these graphs indicate how the feature descriptor is important for classification. Therefore, the feature descriptors with high Mean Decrease Gini value are significant feature descriptors for disease stage classification in this study. As a result of experiments, classification accuracy was 99.8%, when Object-Level features and $m_{try} = 4$ were used.

On the other hand, in the case of VT, classification accuracy was 84.4% ($m_{try} = 4$). In the cases of DT and MST, classification accuracies were 87.1% ($m_{try} = 3$)

Table 4.3: Classification results using SVM and RF.

Features	Type	# of Features	Accuracy (%) (SVM)	Accuracy (%) (RF)
Object-Level Features		21	99.8	99.8
Spatial-Arrangement Features	Voronoi Tessellation	13	84.2	84.4
	Delaunay Triangulation	9	86.5	87.a
	Minimum Spanning Tree	6	87.6	86.8
	All	28	87.8	87.8
Object-Level Features + Spatial-Arrangement Features		49	96.5	99.8

and 86.8% ($m_{try} = 2$), respectively. In the case all Spatial-Arrangement features were used, the classification accuracy was 87.82%, and m_{try} was 6. In addition, the classification accuracy was 99.8%, and m_{try} was 4 when all features were used for classification.

4.2 Discussion

As a result of the evaluation experiment, the Glioma histopathological images were classified accurately with SVM and RF (Table 4.3).

In the case of SVM, the classification accuracy of Object-Level features was higher than that of Spatial-Arrangement features. In addition, the use of the both features decreased classification accuracy by several percents.

In the case of RF, the classification accuracy of Object-Level features was also higher than of Spatial-Arrangement features. In addition, the classification accuracy using the both features was identical with using only Object-Level features. However, Figure 4.2 (3) shows that some Object- Level features had high Mean Decrease Gini value. And in this case, m_{try} was 4. This result indicates that Object-Level features worked well compared to Spatial-Arrangement features for disease stage classification using RF. From these results, when SVM and RF were used as classifiers, using only Object-Level features was reasonable for disease stage classification of Glioma.

As the first reason, it is considered that Spatial-Arrangement features had some

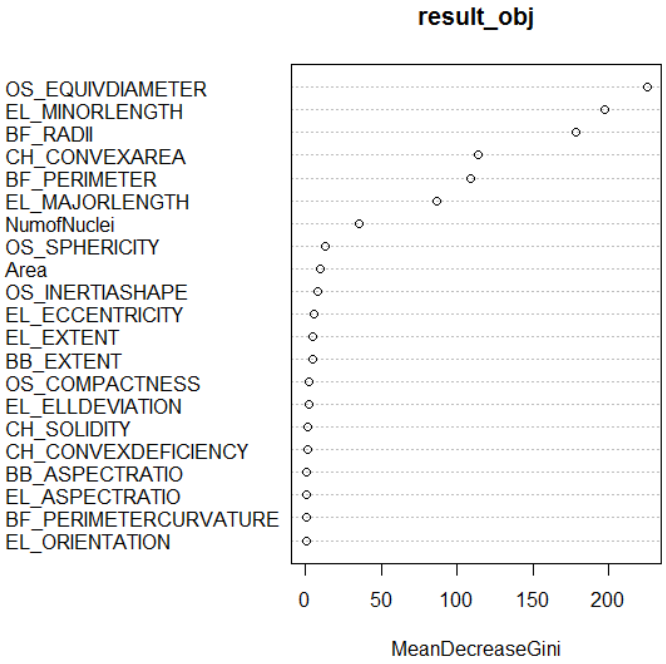

$$Classification Accuracy = 99.8\%$$

(1) Object-Level Features

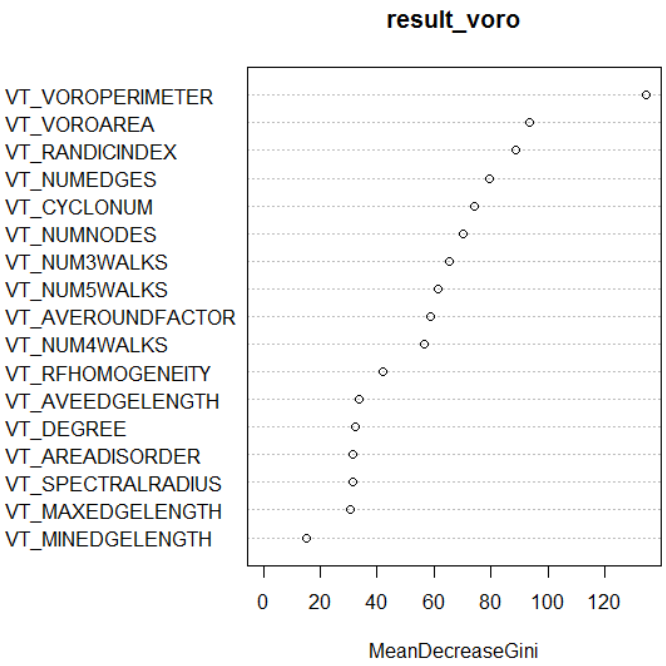

$$Classification Accuracy = 84.4\%$$

(a) Voronoi Tessellation

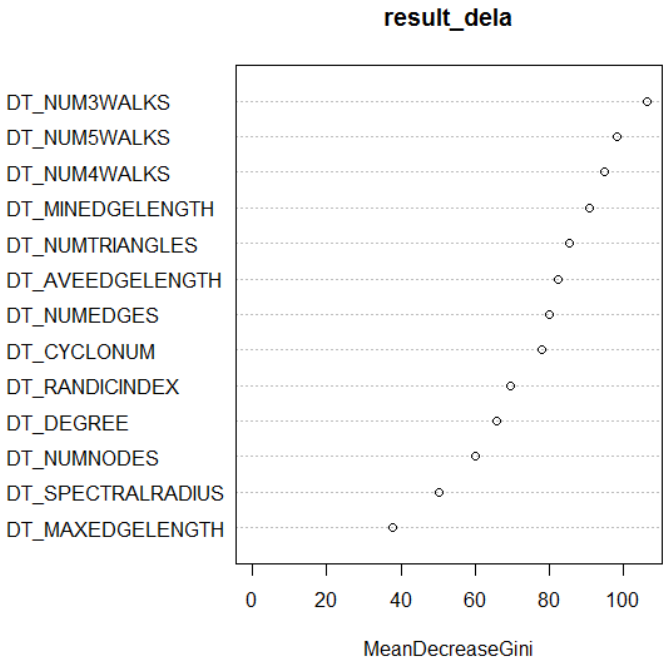

$Classification Accuracy = 87.1\%$

(b) Delaunay Triangulation

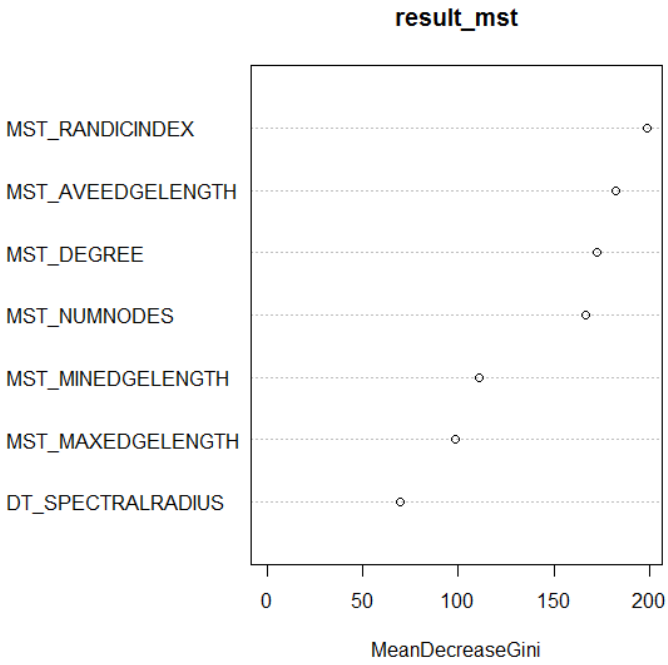

$Classification Accuracy = 86.8\%$

(c) Minimum Spanning Tree

(2) Spatial-Arrangement Features

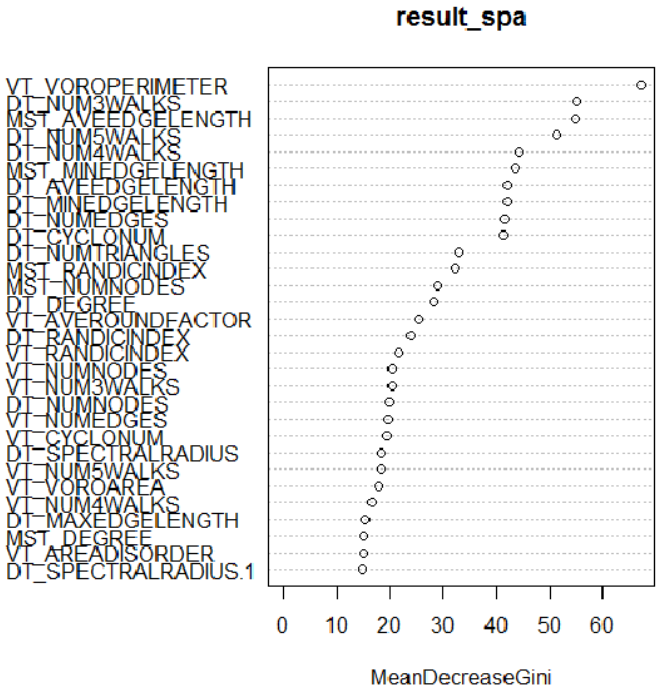

$$Classification Accuracy = 87.8\%$$

(d) All Features of Spatial-Arrangement Features

(2) Spatial-Arrangement Features

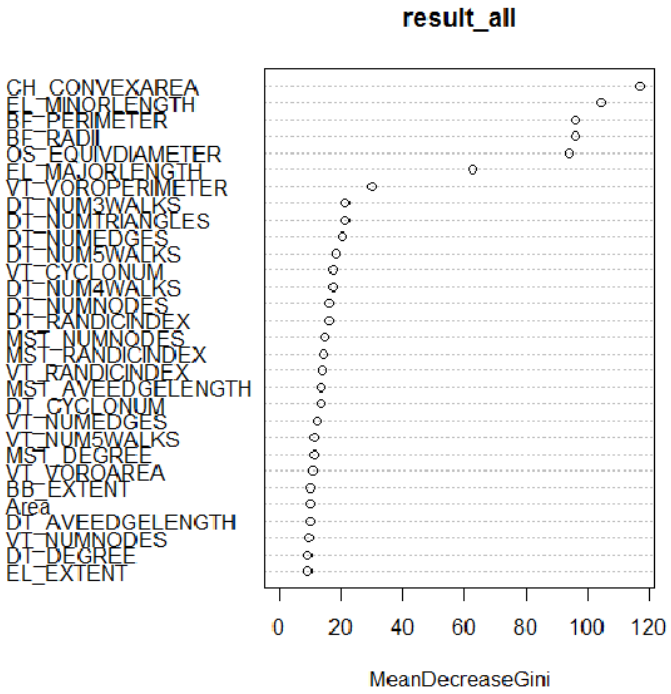

$$Classification Accuracy = 99.8\%$$

(3) Object-Level Features + Spatial-Arrangement Features

Figure 4.2: Graphs of Mean Decrease Gini.

features to reflect the difference of not only disease stage but also each image and these features caused the miss-classification. In the previous research [9], only 1 .svs tissue image was used in each category, and the classification accuracy using SVM and Object-Level features was 98.9%. This value was not different from the accuracy of the proposed method. However, the accuracies of SVM with VT, DT and MST features were 96.2%, 99.4% and 99.0%, respectively. These were quite different from those values in this case. Similarly, the result of classification accuracy using RF and Object-Level features was 100.0%. This accuracy was not different from the accuracy by the current result. On the other hand, the result of classification accuracies using RF with Spatial-Arrangement features (VT, DT, MST) were 99.6%. This value was quite different from the accuracies by the proposed method. From these results, these differences were caused by the number of input images. When Spatial-Arrangement Features were used for a tissue image, the classification accuracies were high. However, the classification accuracies were decreased when 10 tissue images were used. Therefore, Spatial-Arrangement features distinguished not only disease stage but also each image.

As the second reason, these differences might depend how to construct the data-set. In this study, the obtained images from TCGA database were divided small patched images whose sizes were 2000×2000 pixels for quick analysis. However, this step caused the breaking off topological relationships among nodes. Or the patch size was not enough for classification. Therefore, the proposed method could not extract effective Spatial-Arrangement features from the obtained histopathological images completely. And it is thinkable that this point also caused the deterioration of classification accuracies.

Though the data-set construction step has this problem, efficient analysis is required. If the obtained histopathological images were not divided to small patched images, the classification accuracy would be good. However, the analysis will not be done efficiently because of an enormous amount of analysis. From these results, Object-Level features would be better than Spatial-Arrangement features to classify the disease stage of Glioma histopathological images in the TCGA.

Chapter 5

Conclusion and Future Works

5.1 Conclusions

The objective of this study was automatic disease stage classification of Glioma histopathological images. This work discussed nuclei segmentation using custom-designed image processing, a performance of this segmentation method and disease stages classification of Glioma. The images used for analysis in this study were obtained from The Cancer Genome Atlas (TCGA) [11]. Significant feature descriptors for Glioma images were determined and used for classification using Support Vector Machine (SVM) and Random Forests (RF) [10].

After the evaluation experiments, 99.8% of images were classified correctly using SVM and Object-Level features. On the other hand, the results using VT, DT and MST were 84.2%, 86.5% and 87.6%, respectively. And 87.8% of given images were classified correctly when all Spatial-Arrangement features were used. In addition, calcification accuracy was 96.5% in the case all features were used. In the case of RF, classification accuracy was 99.8%, when Object-Level features were employed. On the other hand, when VT, DT and MST were used, classification accuracies were 84.38%, 87.06% and 86.75%, respectively. When all Spatial-Arrangement features were used, the classification accuracy was 87.82%. In addition, the classification accuracy was 99.8% when all features were used for classification.

From there results, in the both of SVM and RF, using only Object-Level features was better than only Spatial-Arrangement features and the both of Object-Level and Spatial-Arrangement features to classify the disease stage of Glioma histological images in the TCGA.

5.2 Future Works

Though dividing to small patched images was important for efficient processing on the target computational platform analysis, the analysis for Spatial-Arrangement features may have been degraded by the division into patch images. Possibly the node graphs of spatial relations could be reattached from one patch to adjacent image patches. This may improve the Glioma classification.

In addition, increasing the number of tissue samples is important for optimization of this method. In this thesis, 10 tissue images were used in each grade. However, more the number of tissue images was required for improvement the proposed method. More experiments with the sufficient number of tissue samples should be conducted.

Another important might be using fuzzy entropy thresholding to improve the overall image analysis pipeline [14], and active contour for improving the accuracy of nuclei segmentation [21]. In this study, the accuracy of the nuclei segmentation method was 86.0%. However, in this literature [22], 96.4% of segmentation accuracy was accomplished by combining the proposed segmentation method with the active contour method [21]. This thesis could not apply this new segmentation method to this disease stage classification, because of much computational time. If the new segmentation method is applied to this classification method, this analysis would be inefficient. The new segmentation method should be optimized and then applied to this problem.

Also another investigation could be to discover disease subtypes using feature matrices and confirm the relationship between the disease stage and results gene expression analysis. I hope the proposed method will be of help in medical decision analysis in general, and brain tumors in particular.

Acknowledgement

First of all, I would like to express the deepest appreciation to Prof. Shinji Tsuruoka who is Executive Vice-President of Mie University, and Associate Prof. Haruhiko Takase, and Associate Prof. Hiroharu Kawanaka at Mie University Graduate School of Engineering, who offered continuing support and constant encouragements.

I am also grateful to Prof. Bruce J. Aronow at Cincinnati Children's Hospital Medical Center and Dr. V. B. Surya Prasath at University of Missouri, USA. They provided a lot of technical help and encouragement. Prof. Aronow accepted me as a short-term study abroad student at his laboratory in Cincinnati Children's Hospital Medical Center. Thanks to his help and encouragement, I was able to make good progress in my project. Dr. Surya gave me a lot of technical and language help in my research project and writing papers.

In addition, this study was partially supported by Mie University study abroad program. Thanks to this program, I could stay Cincinnati Children's Hospital Medical Center for a month to obtain great progress and discuss the project with experts. I would like to sincerely thank this scholarship program.

Finally, I would like to thank other persons who attended to this research project.

Bibliography

[1] M. N. Gurcan, L. E. Boucheron, A. Can, A. Madabhushi, N. M. Rajpoot, and B. Yener, "Histopathological image analysis: A review", IEEE Reviews In Biomedical Engineering, vol. 2, pp. 47–171, 2009.

[2] A. M. Marchevsky and M. R. Wick, "Evidence-based medicine, medical decision analysis, and pathology", Human Pathology, vol. 35, no. 10, pp. 1179–1188, 2004.

[3] L. E. Boucheron, "Object-and spatial-level quantitative analysis of multispectral histopathology images for detection and characterization of cancer", Ph. D. dissertation, University of California, Santa Barbara, CA, 2008.

[4] Bilgin C., Demir C., Nagi C. and Yener B., "Cell-graph mining for breast tissue modeling and classification", Engineering in Medicine and Biology Society, 2007. EMBS 2007. 29th Annual International Conference of the IEEE, pp. 5311-5314, 2007.

[5] K. Rodenacker and E. Bengtsson, "A feature set for cytometry on digitized microscopic images", Analytical Cellular Pathology 25, pp. 1-36, 2003.

[6] O. Sertel, J. Kong, U. V. Catalyurek, G. Lozanski, J. H. Saltz, M. N. Gurcan, "Histopathological Image Analysis Using Model-Based Intermediate Representations and Color Texture: Follicular Lymphoma Grading", J. Signal Process. Syst., vol.55, 169, 2009.

[7] K. Tamaki, K. Fukuma, H. Kawanaka, H. Takase, S. Tsuruoka, B. J. Aronow, and S. Chaganti. "Comparative study on feature descriptors for brain image analysis", International Conference on and Advanced Intelligent Systems (ISIS), Proc. IEEE, pp. 679–682, 2014.

[8] K. Fukuma, H. Kawanaka, V. B. S. Prasath, B. J. Aronow, H. Takase. "Feature extraction and disease stage classification for glioma histopathology images",

IEEE International Conference on E-health Networking, Application & Services (HealthCom), Boston MA, USA, Oct 2015. Proc. IEEE, pp. 429–430.

[9] K. Fukuma, H. Kawanaka, V. B. S. Prasath, B. J. Aronow, H. Takase. "A study on feature extraction and disease stage classification for glioma pathology images", IEEE International Conference on Fuzzy Systems (FUZZ-IEEE), July 2016.

[10] Tin Kam Ho, "Random decision forests" , Third International Conference on Document Analysis and Recognition, vol. 1. Proc. IEEE, pp. 278–282, 1995.

[11] NIH THE CANCER GENOME ATLAS. "https://cancergenome.nih.gov/" (accessed 2016/11/02)

[12] M. R. Lamprecht, D. M. Sabatini, A. E. Carpenter, "CellProfiler: free, versatile software for automated biological image analysis" , Biotechniques, vol. 42, no. 1, pp. 71–75, 2007.

[13] V. B. S. Prasath and R. Delhibabu, "Image restoration with fuzzy coefficient driven anisotropic diffusion" , Joint International Conference on Swarm, Evolutionary and Memetic Computing (SEMCCO), Visakhapatnam, India. Proc. Springer LNCS 8947. (eds. B.K. Panigrahi, P. N. Suganthan, S. Das), pp. 145–155, Dec 2014.

[14] V. B. S. Prasath, R. Delhibabu, "Automatic mucosa detection in video capsule endoscopy with adaptive thresholding" , International Conference on Computational Intelligence in Data Mining (ICCIDM), Bhubaneswar, India. Proc. Springer SIST 410 (Eds.: H. S. Behera, D. P. Mohapatra), pp. 95–102, Dec 2015.

[15] Kiichi Fukuma, Hiroharu Kawanaka, V. B. Surya Prasath, Bruce J. Aronow and Haruhiko Takase, "A Study on Accuracy of Nuclei Segmentation for Tissue Specimen Analysis of Brain Histopathology Images", The Seventh International Workshop on Regional Innovation Studies (IWRIS2015), #6, pp.21-24, 2015

[16] P. J. V. Diest, K. Kayser, G. A. Meijer and J. P. A Baak, "Syntactic structure analysis" , Pathologica, vol. 87, pp. 255-262, 1993.

[17] B. Weyn, W. A. A. Tjalma, P. Vermeylen, A. van Daele, E. va. Marck, and W. Jacob, "Determination of tumour prognosis based on angiogenesis-related vascular patterns measured by fractal and syntactic structure analysis", Clinical Oncology, vol. 16, pp.307-316, 2004.

[18] B. Weyn, G. van de Wouwer, S. Kumar-Singh, A. van Daele, P. Scheunders, E. van Marck, and W. Jacob, “Computer-assisted differential diagnosis of malignant mesothelioma based on syntactic structure analysis”, Cytometry, vol. 35, pp. 23-29. 1999.

[19] J. F. O'Callaghan, “Computing the perceptual boundaries of dot patterns”, Computer Graphics and Image Processing, vol. 3, pp. 141-162, 1974.

[20] R. Marcelpoil and Y. Usson, “Methods for the study of cellular sociology: Voronoi diagrams and parametrization of the spatial relationships”, Journal of Theoretical Biology, vol. 154, pp. 359-369, 1992.

[21] V. B. S. Prasath, K. Fukuma, B. J. Aronow, and H. Kawanaka, “Cell nuclei segmentation in glioma histopathology images with color decomposition based active contours”, IEEE International Conference on Bioinformatics and Biomedicine (BIBM), Washington, DC, USA. Proc. IEEE, pp. 1734–1736, Nov 2015.

[22] Kiichi Fukuma, Hiroharu Kawanaka, V. B. Surya Prasath, Bruce J. Aronow and Haruhiko Takase, “A Proposal of New Segmentation Method for Glioma Pathology Images”, The Eighth International Workshop on Regional Innovation Studies (IWRIS2016), #8, pp.42-45, 2016

Publication List

International Conferences

1. Kiichi Fukuma, Hiroharu Kawanaka, V. B. Surya Prasath, Bruce J. Aronow and Haruhiko Takase: Feature Extraction and Disease Stage Classification for Glioma Histopathology Images, 17th International Conference on E-health Networking, Application & Services (HealthCom), pp. 598-599, 2015

2. Kiichi Fukuma, Hiroharu Kawanaka, V. B. Surya Prasath, Bruce J. Aronow and Haruhiko Takase: A Study on Feature Extraction Method from Histopathology Images for Disease Progress Analysis, 5th International Symposium for Sustainability by Engineering at Mie University (Research Area C) (IS2EMU2015-C), A-13, pp. 26-27, 2015

3. Kiichi Fukuma, Hiroharu Kawanaka, V. B. Surya Prasath, Bruce J. Aronow and Haruhiko Takase: A Study on Accuracy of Nuclei Segmentation for Tissue Specimen Analysis of Brain Histopathology Images, 7th International Workshop on Regional Innovation Studies (IWRIS2015), #6, pp. 21-24, 2015

4. V. B. Surya Prasath, Kiichi Fukuma, Bruce J. Aronow and Hiroharu Kawanaka: Cell nuclei segmentation in glioma histopathology images with color decomposition based active contours, IEEE International Conference on Bioinformatics and Biomedicine (BIBM), pp. 1734–1736, 2015

5. Kiichi Fukuma, V. B. Surya Prasath, Hiroharu Kawanaka, Bruce J. Aronow and Haruhiko Takase: A Study on Feature Extraction and Disease Stage Classification for Glioma Pathology Images, IEEE International Conference on Fuzzy Systems (FUZZ-IEEE), pp. 2150-2156, 2016

6. Kiichi Fukuma, V. B. Surya Prasath, Hiroharu Kawanaka, Bruce J. Aronow and Haruhiko Takase: A study on nuclei segmentation, feature extraction and disease stage classification for human brain histopathological images, 20th

International Conference on KnowledgeBased and Intelligent Information & Engineering Systems (KES-2016), pp. 1202-1210, 2016

7. Kiichi Fukuma, Hiroharu Kawanaka, V. B. Surya Prasath, Bruce J. Aronow and Haruhiko Takase: Nuclei Segmentation and Feature Extraction for Automatic Classification of Glioma Histopathology Images, 6th International Symposium for Sustainability by Engineering at Mie University (Research Area C) (IS2EMU2016-C), B-1, pp. 41-42, 2016

8. Kiichi Fukuma, Hiroharu Kawanaka, V. B. Surya Prasath, Bruce J. Aronow and Haruhiko Takase: A Proposal of New Segmentation Method for Glioma Pathology Images, 8th International Workshop on Regional Innovation Studies (IWRIS2016), #8, pp. 42-45, 2016

Domestic Conferences

1. 福間貴一，川中普晴，V. B. Surya Prasath，Bruce J. Aronow，高瀬治彦，“脳組織病理画像を用いた疾患の進行度評価のための特徴量抽出に関する一検討”，第 31 回ファジィシステムシンポジウム FSS2015 in 調布講演論文集，TD2-2 pp. 540-543，2015

2. 福間貴一，川中普晴，V. B. Surya Prasath，Bruce J. Aronow，高瀬治彦，“Glioma の組織病理画像を用いた進行度評価のための特徴量抽出とその比較に関する一検討”，平成 27 年度電気・電子・情報関係学会東海支部連合大会講演論文集，N1-7，2015

3. 福間貴一，川中普晴，V. B. Surya Prasath，Bruce J. Aronow，高瀬治彦，鶴岡信治，“脳組織病理画像を対象とした Glioma の疾患進行度評価システムの開発”，地域イノベーション学会誌 (Journal of the Society for Regional Innovation Studies), Volume 4, pp. 39, 2015

4. 福間貴一，川中普晴，V. B. Surya Prasath，Bruce J. Aronow，高瀬治彦，“Glioma を対象とした疾患進行度推定に関する研究”，アカデミックフェア 2016

5. 福間貴一，川中普晴，V. B. Surya Prasath，Bruce J. Aronow，高瀬治彦，“Glioma の進行度評価のための細胞核領域抽出，特徴量抽出とその比較に関する検討”，平成 28 年度電気・電子・情報関係学会東海支部連合大会講演論文集，D4-6，2016

6. 福間貴一，川中普晴，V. B. Surya Prasath，Bruce J. Aronow，高瀬治彦，鶴岡信治，“脳組織病理画像を対象とした細胞核領域抽出法の提案”，地域イノ

ベーション学会誌 (Journal of the Society for Regional Innovation Studies), Volume 5, pp. 43, 2016